AGU PUBLICATIONS

JGR

Journal of Geophysical Research: Atmospheres

RESEARCH ARTICLE
10.1002/2014JD021872

Key Points:
- We implement modified Richards equation into the regional climate model RegCM4
- Impact of modified Richards equation on simulated summer precipitation is mixed
- The modified numerical method improves the ground water table depth simulations

Correspondence to:
Z. Xie,
zxie@lasg.iap.ac.cn

Citation:
Yu, Y., Z. Xie, and X. Zeng (2014), Impacts of modified Richards equation on RegCM4 regional climate modeling over East Asia, *J. Geophys. Res. Atmos.*, *119*, 12,642–12,659, doi:10.1002/2014JD021872.

Received 9 APR 2014
Accepted 16 OCT 2014
Accepted article online 21 OCT 2014
Published online 28 NOV 2014

Impacts of modified Richards equation on RegCM4 regional climate modeling over East Asia

Yan Yu[1,2], Zhenghui Xie[1], and Xubin Zeng[3]

[1]State Key Laboratory of Numerical Modeling for Atmospheric Sciences and Geophysical Fluid Dynamics, Institute of Atmospheric Physics, Chinese Academy of Sciences, Beijing, China, [2]Zhejiang Institute of Meteorological Sciences, Hangzhou, China, [3]Department of Atmospheric Sciences, University of Arizona, Tucson, Arizona, USA

Abstract To remove the deficiency of the numerical solution of the mass conservation-based Richards equation for soil moisture in a regional climate model (RegCM4 with its land surface component Community Land Model 3.5 (CLM3.5)), a revised numerical algorithm that is used in CLM4.5 is implemented into CLM3.5. Compared with in situ measurements, the modified numerical method improves the ground water table depth simulations in RegCM4. It also improves the temporal and spatial variability of soil moisture to some extent. Its impact on simulated summer precipitation is mixed, with improvements over three subregions in China but with increased errors in three other subregions. The impact on the simulated summer temperature is relatively small (with the mean biases changed by less than 10% over most subregions). The evapotranspiration differences between modified and control land-atmosphere coupled simulations are enhanced over the northwest subregion and Tibetan Plateau compared to offline simulations due to land surface feedbacks to the atmosphere (in coupled simulations). Similarly the soil moisture differences in coupled simulations are geographically different from those in offline simulations over the eastern monsoon area. The summer precipitation differences between modified and control coupled simulations are found to be explained by the differences of both surface evapotranspiration and large-scale water vapor flux convergence which have opposite signs over the northwest subregion and Tibetan Plateau but have the same signs over other subregions.

1. Introduction

Soil moisture, as an important part of the hydrologic cycle, is a crucial factor in land-atmosphere interactions. Its slow evolution is driven by atmospheric forcing, especially by precipitation [*Koster et al.*, 2004; *Guo et al.*, 2006; *Wang and Zeng*, 2011]. On the other hand, variations in horizontal and vertical soil moisture patterns change atmospheric boundary layer structures by directly modifying evapotranspiration and heat fluxes and ultimately influence convection and large-scale circulation patterns [*Milly*, 1992; *Cuenca et al.*, 1996; *Schar et al.*, 1999; *Timbal et al.*, 2002; *Kim and Hong*, 2007; *Yuan et al.*, 2008a]. The impacts of soil moisture conditions on subsequent precipitation in seasonal climate prediction have been documented by observations and model simulations [*Eltahir*, 1998; *Yang et al.*, 2004; *Kim and Hong*, 2007]. Hence, an accurate computation of soil moisture plays a significant role in climate modeling and prediction.

The vertical distribution of soil moisture is generally described by soil-water balance equations such as the physically based Richards equation [*Richards*, 1931]. Surface infiltration, evapotranspiration, and runoff are the sources and sinks of the soil water conservation model. Therefore, the vertical movement of soil water is regulated by the upper and lower boundary conditions of a soil column, by vegetation types providing root fractions for transpiration, by the hydraulic properties of the soil which determine the soil matric potential and hydraulic parameters, and by the soil water phase and other factors. Studies on the impacts of these factors on soil moisture, atmospheric boundary layer, and regional and global climate have provided vital insights [*Segal et al.*, 1998; *LeMone et al.*, 2007; *Pielke et al.*, 2007; *Gao et al.*, 2008a, 2008b; *Niu et al.*, 2011; *Tawfik and Steiner*, 2011; *Chen and Xie*, 2012]. Many efforts have also been made to improve the simulation of soil water movement in land surface and climate models by incorporating groundwater as the models' lower boundary condition to investigate land-atmosphere interactions [*Liang et al.*, 2003; *Niu et al.*, 2007; *Fan et al.*, 2007; *Miguez-Macho et al.*, 2007; *Anyah et al.*, 2008; *Yuan et al.*, 2008a; *Maxwell et al.*, 2011; *Miguez-Macho and Fan*, 2012; *Tian et al.*, 2012]. Another key factor in soil water calculations is the numerical solution of the soil water equation.

Numerical solutions of the soil-water conservation equation in current land surface models, including those used in most of the studies mentioned above, are often accompanied by gravitational drainage or zero flux as

the lower boundary condition [*Dickinson et al*., 1993; *Sellers et al*., 1996; *Chen and Dudhia*, 2001; *Mitchell et al*., 2004; *Oleson et al*., 2004, 2008]. *Zeng and Decker* [2009] pointed out that traditional numerical solution of the Richards equation results in large truncation errors in regions with a shallow water table and relatively small errors in regions with a deep water table because the equilibrium state cannot be maintained in the integration. Consequently, they subtracted the hydrostatic equilibrium soil moisture distribution from the original form of the equation with a corresponding nonzero lower boundary condition to reduce truncation errors substantially. Meanwhile, *Decker and Zeng* [2009] obtained better performance for terrestrial water and energy cycles using the Community Land Model 3.5 (CLM3.5) by implementing this improved numerical algorithm of the Richards equation together with other improvements in water table depth, subsurface drainage, and surface runoff modeling. Subsequently, this modified Richards equation has been used by CLM4.0 and CLM4.5 as a part of comprehensive improvements to the model [*Lawrence et al*., 2011, 2012]. However, the effects of the revised numerical algorithm for the Richards equation on regional climate simulations have not yet been studied, and the detailed regional characteristics of the impacts of this modification is not clear.

In this study, the modified form of the Richards equation is implemented with its new lower flux boundary condition as developed by *Zeng and Decker* [2009] in the regional climate model RegCM4 with its land surface component CLM3.5 to investigate its potential effects on regional climate simulations over East Asia. This research focuses on regional characteristics and homologous reasons for the effects in different climatic regions. To help interpret the results from the land-atmosphere coupled RegCM4 model, offline CLM3.5 simulations will also be carried out.

This paper is organized as follows. Section 2 describes the regional climate model, the land surface model with the original and modified numerical solutions of the Richards equation, and the data used in this study. Section 3 introduces the experimental design. The effects of the revised numerical method on regional climate simulations of land-atmosphere interactions are illustrated in section 4. Finally, section 5 presents a summary.

2. Model and Data Description

2.1. Regional Climate Model RegCM4

The latest version of the Abdus Salam International Center for Theoretical Physics Regional Climate Model (RegCM4) described by *Giorgi et al*. [2012] is used in this study. RegCM4 has a hydrostatic dynamic core based on the hydrostatic calculations of Mesoscale Model version 5 [*Grell et al*., 1994] on an Arakawa B horizontal grid and a terrain following sigma *p* vertical coordinate. Some remarkable improvements have been included in this version, such as the coupling of an advanced and complex land surface model (CLM3.5) [*Oleson et al*., 2008].

Compared to its previous version, RegCM3 [*Pal et al*., 2007], RegCM4 includes major upgrades to the structure of the code and its preprocessors and postprocessors and offers a series of new schemes, including aerosol radiative transfer calculations, planetary boundary layer processes, a mixed convection scheme, and a diurnal sea surface temperature scheme. The RegCM model has been applied to East Asia for a wide range of studies such as modern-day climate validation against observations, land cover change, land-atmosphere interactions, and future climate change [*Liu et al*., 1994; *Giorgi et al*., 1999, 2012; *Yuan et al*., 2008a; *Chen and Xie*, 2010, 2012; *Gao et al*., 2002, 2006, 2008a, 2008b, 2011, 2012; *Wu*, 2012; *Yu and Xie*, 2013; *Li et al*., 2013].

2.2. Land Surface Model CLM 3.5 With Revised Formulation of the Richards Equation

Spatial land surface heterogeneity in CLM3.5 is represented as a nested subgrid hierarchy in which grid boxes are composed of multiple land units, snow/soil columns, and plant function types. Up to five snow layers and 10 soil layers are used, with an unconfined aquifer vertically distributed. New surface data sets based on the Moderate Resolution Spectroradiometer products [*Lawrence and Chase*, 2007] and parameterizations such as a simple groundwater model for determining water table depth were implemented by *Niu et al*. [2007] into CLM3.5 [*Oleson et al*., 2004] as improvements over CLM3. Vertical soil water movement is governed by the Richards equation:

$$\frac{\partial \theta}{\partial t} = \frac{\partial}{\partial z}\left[K\frac{\partial(\psi + z)}{\partial z}\right] - e, \tag{1}$$

$$q = -K\frac{\partial(\psi + z)}{\partial z}, \tag{2}$$

where θ is the volumetric soil water content, t is time, z is height above some datum in the soil column, q is soil water flux between two adjacent layers based on Darcy's law, and e is a soil moisture sink term derived from evapotranspiration loss. The z and q are positive upwards, K is the hydraulic conductivity between two adjacent layers, and ψ is the soil matric potential. CLM3.5 uses zero flux between the bottom soil layer (3.43 m) and groundwater to solve equations (1) and (2) numerically and then couples the groundwater with the soil layers by means of the recharge rate.

Zeng and Decker [2009] found a deficiency in the soil-water conservation numerical solution for equation (1) for saturated soil layers with a shallow water table. The integration in equation (1) cannot maintain the hydrostatic equilibrium state of soil water and results in significant truncation errors when the water table is within the model domain and relatively small errors only when the water table is below the model domain. *Zeng and Decker* [2009] subtracted the equilibrium state of soil moisture from the Richards equation with a corresponding lower flux boundary condition to remove the deficiencies of the numerical scheme for both shallow and deep water tables. The revised Richards equation can be stated as

$$\begin{aligned}\frac{\partial\theta}{\partial t} &= \frac{\partial}{\partial z}\left[K\frac{\partial(\psi+z-C)}{\partial z}\right]-e\\ &= \frac{\partial}{\partial z}\left[K\frac{\partial(\psi+z-(\psi_E+z))}{\partial z}\right]-e,\\ &= \frac{\partial}{\partial z}\left[K\frac{\partial(\psi-\psi_E)}{\partial z}\right]_e \end{aligned} \tag{3}$$

$$q = -K\frac{\partial(\psi-\psi_E)}{\partial z}, \tag{4}$$

where C is a constant hydraulic potential and ψ_E is the equilibrium soil matric potential based on an empirical function proposed by *Clapp and Hornberger* [1978]:

$$\begin{aligned}\psi_E &= \psi_{\text{sat}}\left(\frac{\theta_E(z)}{\theta_{\text{sat}}}\right)^{-B},\\ &= C-z=\psi_{\text{sat}}+z_\nabla-z\end{aligned} \tag{5}$$

where z_∇ is the water table depth. The layer average θ_j can be obtained by integrating $\theta_E(z)$ for layer j using equation (5), following which ψ_E for each layer can be computed. An extra soil layer between the lowest soil layer and the water table in CLM3.5 was added to the bottom of the soil column. The soil water flux between the tenth and eleventh layers, computed as in equation (4), becomes the new lower boundary condition for numerical solution of the Richards equation instead of the previous zero-flux condition. Hence, the modified numerical algorithm directly couples the soil column of 11 layers with the aquifer. The calculation of water table depth still uses the original algorithm in CLM3.5. When the water table (z_∇) is below the soil column, the water table depth is proportional to the water stored in the aquifer W_a:

$$\frac{\mathrm{d}W_a}{\mathrm{d}t} = q_{\text{rechar}}-q_{\text{drai}},\quad z_\nabla = z_{h,10}+25-\frac{W_a}{10^3 S_y}, \tag{6}$$

where $z_{h,10}$ is the bottom of the soil column (3.43 m), S_y is the specific field, q_{rechar} is the recharge to the aquifer, and q_{drai} is the subsurface runoff. When the water table is within the soil column, the water table depth is determined by the water stored in the soil and the aquifer W_t and effective porosity θ_{eff}:

$$\frac{\mathrm{d}W_t}{\mathrm{d}t} = q_{\text{rechar}}-q_{\text{drai}},\quad z_\nabla = \begin{cases} z_{h,i+1}-\dfrac{W_t-10^3\cdot 25S_y-\sum_{j=i+2}^{10}\Delta z_j\theta_{\text{eff},j}}{10^3\theta_{\text{eff},i+1}} & 1\le i\le 8\\ z_{h,i+1}-\dfrac{W_t-10^3\cdot 25S_y}{10^3\theta_{\text{eff},i+1}} & i=9\end{cases}. \tag{7}$$

2.3. Data Description

In situ observations of soil moisture from 778 agriculture-meteorology stations over mainland China are obtained from the China Meteorological Data Sharing Service system. Relatively continuous and long-term

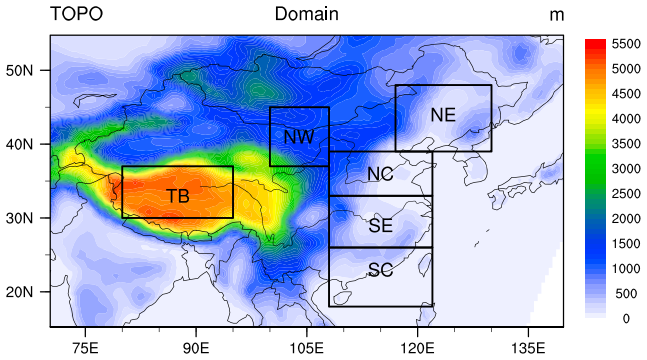

Figure 1. Study domain with elevation distribution (NE = northeast China, NC = north China, SE = southeast China, SC = south China, TB = Tibetan Plateau, NW = northwest region).

measurements at 226 stations at soil depth of 10 cm, 20 cm, and 100 cm are used to evaluate the model simulations in this study. This soil moisture observation data set has been widely used in assessing and improving simulation of soil moisture in China [*Liu et al*., 2001; *Li et al*., 2005; *Wang and Zeng*, 2011; *Liu and Xie*, 2013]. As zoned into subregions in Figure 1, approximately 32 and 7 observational sites are available from April to September over the NE and NW subregions, respectively. More than 60 sites are available in all months except January over NC. Twenty-six sites and only three sites are available over the SE and SC subregions, respectively. However, there are no observational sites over TB. The monthly data of water table depths from 572 monitoring wells, supplied by the Ministry of Water Resources and Institute for Geo-Environmental Monitoring in China, are compiled by *Yuan et al*. [2008b].

Observational precipitation data set from a gauge-based analysis of daily precipitation over East Asia by interpolating station observations at over 2200 gauges [*Xie et al*., 2007] is used to assess modeled precipitation bias. Climatic Research Unit Time Series 3.0 (CRU TS3.0) global temperature data set [*Mitchell and Jones*, 2005] is used in modeled temperature evaluation. Both data sets are on a 0.5° latitude-longitude grid and widely used in evaluating dynamically downscaled outputs and regional climate model performance [*Yuan et al*., 2008a; *Chen and Xie*, 2012; *Liu et al*., 2013; *Wu and Zhang*, 2013; *Syed et al*., 2014].

The Princeton forcing data set based on the National Centers for Environmental Prediction-National Center for Atmospheric Research reanalysis, in situ measurement, and remote sensing [*Sheffield et al*., 2006] is applied to drive offline CLM3.5 simulations. Its precipitation is adjusted based on in situ and satellite measurements (i.e., CRU TS2.0, Global Precipitation Climatology Project, and Tropical Rainfall Measuring Mission data sets), while its 2 m air temperature is adjusted using the in situ CRU TS2.0 data set. Many studies carried out offline CLM simulations forced by the Princeton forcing data to analyze soil moisture, soil temperature, and terrestrial water cycle in China [*Li and Ma*, 2010; *Chen et al*., 2010; *Xiong et al*., 2011; *Wang and Zeng*, 2011; *Lai et al*., 2014].

3. Experimental Design

The study domain of land-atmosphere coupled RegCM4 simulations includes continental China and its surrounding areas and is centered at 36°N/102°E, with a grid size of 60 km and 120 × 90 grid points (Figure 1). There are 18 vertical levels with 50 hPa at the model top. Two experiments are conducted: (1) a baseline run (denoted as RCTL) with the original RegCM4/CLM3.5 model and (2) a comparative run (denoted as RMOD), in which the revised numerical algorithm for the Richards equation is used. Each simulation uses the European Centre for Medium-Range Weather Forecasts 40 year reanalysis data sets [*Uppala et al*., 2005] and the National Oceanic and Atmospheric Administration optimally interpolated sea surface temperatures [*Reynolds et al*., 2002] as initial and lateral boundary conditions. The Grell scheme [*Grell*, 1993] with Fritsch and Chappell closure [*Fritsch and Chappell*, 1980] is used as the cumulus convective scheme. The 6-hourly lateral boundary fields use exponential relaxation techniques [*Davies and Turner*, 1977]. Both simulations are conducted from 1 January 1982 to 1 January 2002 with a time step of 120 s; the first 11 years are considered as spin-up, and the last 9 years (1993–2001) are selected for analysis.

To help interpret the results from RegCM4/CLM3.5, CLM3.5 will also be used for offline simulations over the same domain. Two experiments are conducted: (1) a control run (denoted as LCTL) with the CLM3.5 standard package and (2) a comparative run (denoted as LMOD) with the modified numerical solution of the Richards equation described in section 2.2 and implemented in CLM3.5. The global meteorological forcing data set [*Sheffield et al*., 2006] is used to drive the control run at 0.5° spatial resolution over China from 1948 to 1992.

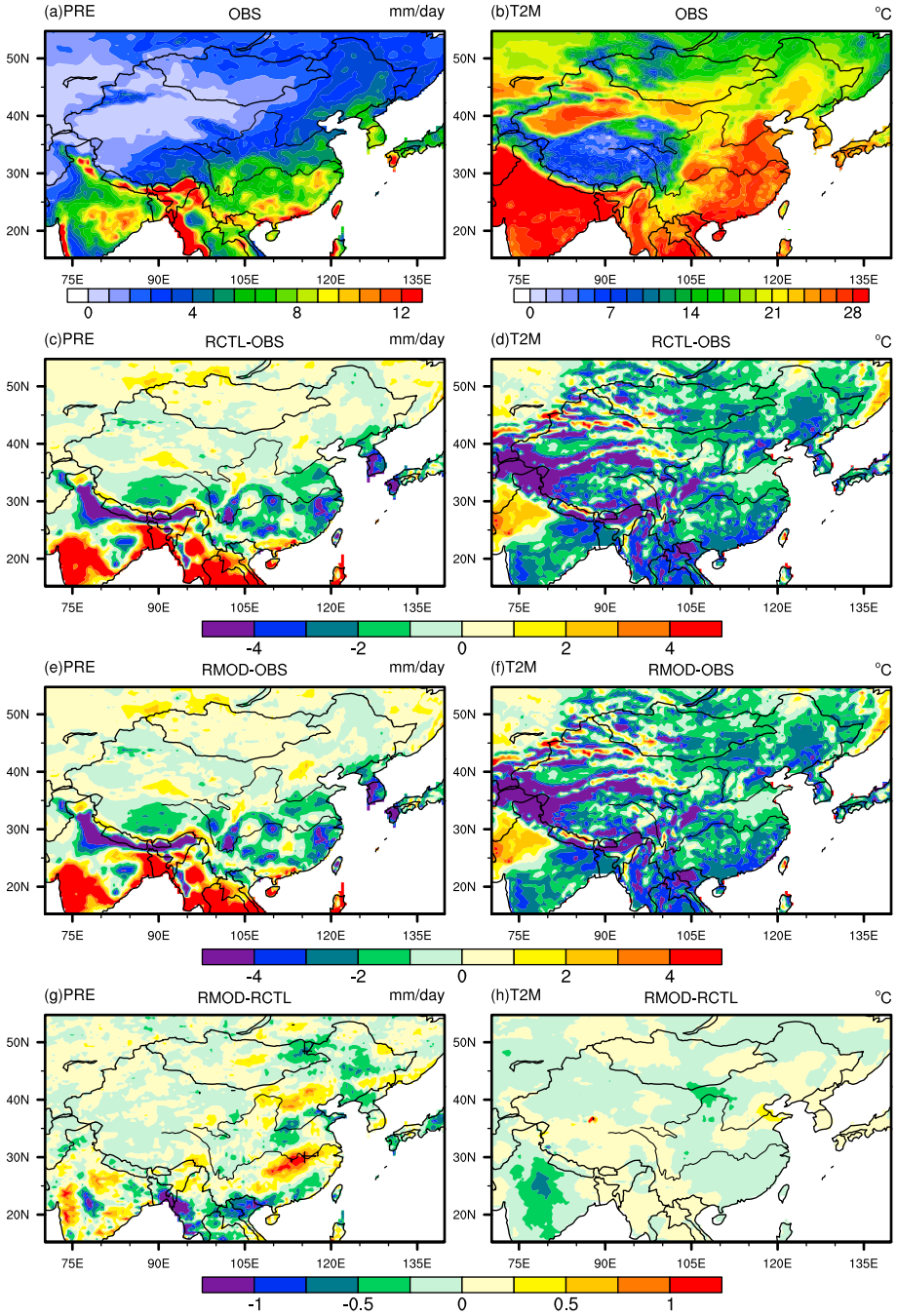

Figure 2. (a, b) Mean precipitation (mm/d) and 2 m air temperature (℃) (1993–2001) in JJA from observations, (c, d) differences between RCTL and observations, (e, f) differences between RMOD and observations, and (g, h) differences between RMOD and RCTL. Note that the color bars differ for various panels.

Then the restart file on 1 January 1993 is used as initial conditions to run both simulations from 1993 to 2001. Note that both coupled simulations use the offline CLM land state on 1 January 1982 simulated by the LCTL run as the initial land condition including soil water, soil ice, soil temperature, and snow water, in order to eliminate the disparity of balanced status between offline and coupled simulations. Also note that the same atmospheric model (RegCM4) is used in both RCTL and RMOD to facilitate the impact study in this paper, even though part of the atmospheric model might be retuned for the production run when the land model is improved.

Table 1. Statistics (Mean Error, Mean Absolute Error, and Correlation Coefficient) of JJA Mean Precipitation (mm/d) and 2 m Air Temperature (°C) From RMOD and RCTL Simulations in Comparison With Observations[a]

		NE		NC		SE		SC		TB		NW	
		RCTL	RMOD	RCTL	RMOD	RCTL	RMOD	RCTL	RMOD	RCTL	RMOD	RCTL	RMOD
PRE	ME	−0.27	−0.37	−0.53	−0.63	−1.68	−1.37	0.30	0.21	−0.56	−0.61	−0.07	−0.05
		(−6.8%	−9.2%	−13.5%	−16.1%	−24.7%	−20.2%	3.2%	2.2%	−29.2%	−31.5%	−6.2%	−4.2%)
	MAE	0.54	0.53	0.77	0.85	1.77	1.58	2.39	2.42	0.92	0.94	0.21	0.23
	CC	0.73	0.69	0.48	0.43	0.55	0.50	0.46	0.44	0.54	0.56	0.92	0.91
T_{2M}	ME	−2.0	−2.0	−1.2	−1.1	−2.0	−2.1	−2.7	−2.7	−3.1	−3.0	−1.3	−1.4
	MAE	2.1	2.1	1.3	1.3	2.0	2.1	2.9	2.9	3.1	3.1	1.5	1.7
	CC	0.88	0.88	0.87	0.88	0.81	0.81	0.58	0.58	0.74	0.75	0.94	0.94

[a]The relative mean errors are given in parentheses.

For convenience of analysis, six subregions are chosen based on the climate shown in Figure 1. The northeastern (NE) subregion has a semihumid climate, while the northern (NC) subregion has a semiarid climate. The southeastern (SE) subregion represents a humid climate and contains the middle and lower reaches of the Yangtze River Basin. The humid southern (SC) subregion is located in the coastal area and receives abundant rainfall. The other two subregions are the Tibet Plateau (TB) and the arid northwest (NW) in the middle of East Asia. East Asia is a typical monsoon region with pronounced seasonality, and soil moisture-rainfall feedback is most significant in summer. Hence, the analysis described below is focused on land surface and atmospheric processes in summer.

4. Impacts of the Modified Richards Equation on Regional Climate Simulation

4.1. Precipitation and 2 m Air Temperature

The June, July and August (JJA) mean precipitation and 2 m air temperature over East Asia from observations [*Xie et al*., 2007; *Mitchell and Jones*, 2005], differences between simulations and observations, and differences between the RMOD and RCTL runs are shown in Figure 2. In addition, Table 1 lists detailed statistics for both variables. The RCTL run underestimates precipitation over most areas of China including south of lower and middle reaches of Yellow River and southern Tibetan Plateau and overestimates precipitation in south China (Figure 2c). The RMOD run alleviates the underestimation of RCTL over the middle and lower reaches of Yangtze River and the overestimation of RCTL in south China and northeast Plain but does not show better performance in northern China and southern Tibetan Plateau (Figure 2g). The differences between RMOD and RCTL are significant at the 95% level over the middle reach of Yangtze River only.

Accordingly RMOD performs better than RCTL over the SE, SC, and NW subregions with regard to the systematic error (ME) (Table 1). The relative variations of ME calculated by $\frac{|ME_{RMOD}|-|ME_{RCTL}|}{|ME_{RCTL}|}\times 100\%$ over these three subregions are −18.5%, −31.5%, and −32.6%, respectively. But MEs in the other three subregions get worse (34.5%, 19.7%, and 7.9%). Regarding the mean absolute error (MAE), RMOD performs better over SE, while RCTL performs better at NC. They have similar performances over other subregions. All the spatial correlation coefficients (CC) of precipitation between the two simulations and observations are significant at the 95% confidence level, but the CC differences are not significant.

Using similar climatic zoning, *Yuan et al*. [2008a] found that the differences resulting from incorporating water table dynamics in the summer of 2000 range from −0.9 to 0.1 mm/d and the relative variations of ME range from −50% to 5.6%. *Chen and Xie* [2012] showed that changes in precipitation due to crop growth and development are −0.22 to −0.01 mm/d and the relative variations of ME range from −23.8% to 3.2%. *Zou and Xie* [2012] applied CLM instead of another land model (Biosphere-Atmosphere Transfer Scheme) in RegCM4 and found −0.3 to −0.09 mm/d differences in precipitation over subregions. The precipitation differences of −0.10 to 0.31 mm/d due to the modified Richards equation in this study, and the relative variations of ME of −32.6% to 34.5% over subregions are similar in magnitude to these previous studies.

RCTL generally underestimates the temperature over China (Figure 2d), while RMOD slightly alleviates this cold bias over northeast and north China and Tibetan Plateau (Figure 2h). The spatial changes in 2 m air

Table 2. Statistics (Mean Error, Mean Absolute Error, and Correlation Coefficient) of JJA Mean Precipitation (mm/d) and 2 m Air Temperature (℃) From the Princeton Forcing Data Set [*Sheffield et al.*, 2006] in Comparison With Observations

		NE	NC	SE	SC	TB	NW
PRE	ME	0.30	0.10	−0.79	−0.49	0.38	0.17
		(7.6%	2.6%	−11.6%	−5.3%	19.8%	15.1%)
	MAE	0.59	0.37	1.09	1.55	0.92	0.40
	CC	0.78	0.85	0.64	0.53	0.63	0.66
T_{2M}	ME	−0.06	−0.05	0.02	−0.03	−0.12	−0.11
	MAE	0.40	0.47	0.48	0.61	0.97	0.60
	CC	0.97	0.96	0.90	0.78	0.87	0.96

temperature due to the modified Richards equation over most regions of study domain do not pass the statistical significance test at the 95% confidence level. Changes in ME of the six subregions are within 0.2℃ (Table 1). All the spatial correlation coefficients (CC) of 2 m air temperature between the two simulations and observations are significant at the 95% confidence level, but differences in the correlation coefficients (CC) over all the subregions are not significant.

To help interpret the above results, Table 2 shows the detailed statistics of precipitation and surface air temperature from the Princeton atmospheric forcing data set used in offline simulations. The Princeton forcing data set essentially represents the uncertainties of observational data sets from different sources. Since the CRU TS3.0 temperature data set [*Mitchell and Jones*, 2005] is used as our validation data set, the temperature agreements in Table 2 (essentially between two versions of the CRU temperature data) are much higher than those in Table 1 (between model results and observations). In contrast, the precipitation differences between the two data sets in Table 2 are comparable to those between models and observations over some subregions (NE, SC, and NW) in Table 1.

4.2. Soil Moisture

JJA mean soil moisture values from observations and the RCTL run and the differences between the RMOD and RCTL runs are shown in Figure 3. Both RCTL and RMOD runs capture the spatial pattern of JJA mean soil moisture with a northwest-to-southeast gradient compared to observations in each observed layer, while RCTL overestimates soil moisture over northeastern and northern China (Figures 3b and 3f). RMOD reduces the overestimation over the northeast plain and north China, to some extent. In addition, RMOD decreases soil moisture over most areas of the Tibetan Plateau, making the soil moisture bias slightly worse over the northwestern corner of the Plateau. However, it increases soil moisture over the southern edge of the Plateau,

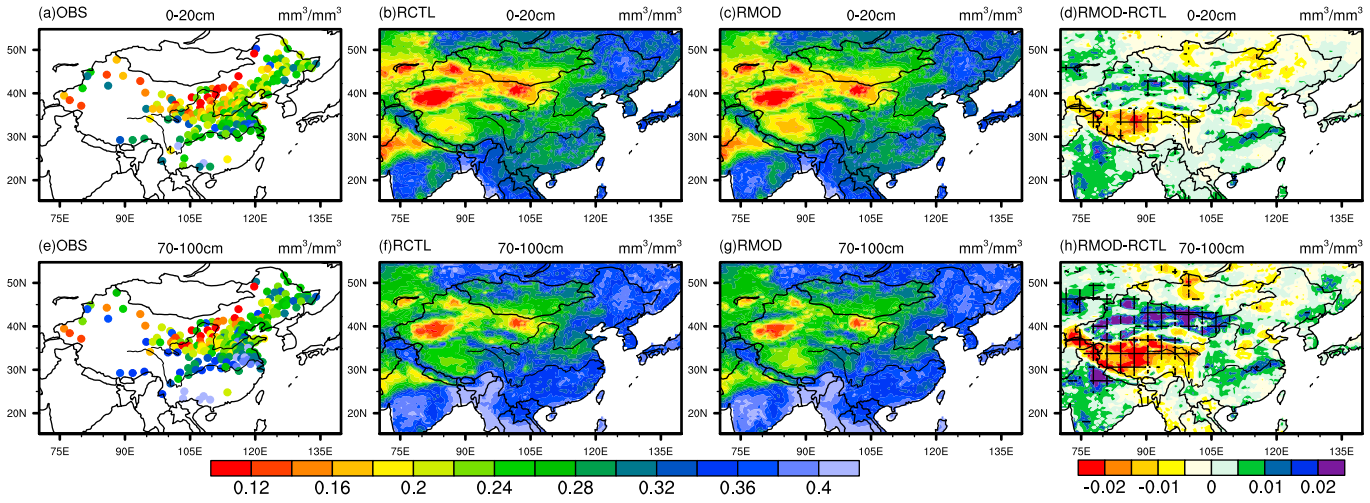

Figure 3. Mean volumetric soil moisture (mm^3/mm^3) (1993–2001) in JJA in 0–20 cm and 70–100 cm from (a, e) observations, (b, f) RCTL, (c, g) RMOD, and (d, h) RMOD − RCTL. Note that the color bars for Figures 3d and 3h differ from those for other panels, and the differences are significant at the 95% confidence level over hatched areas in Figures 3d and 3h.

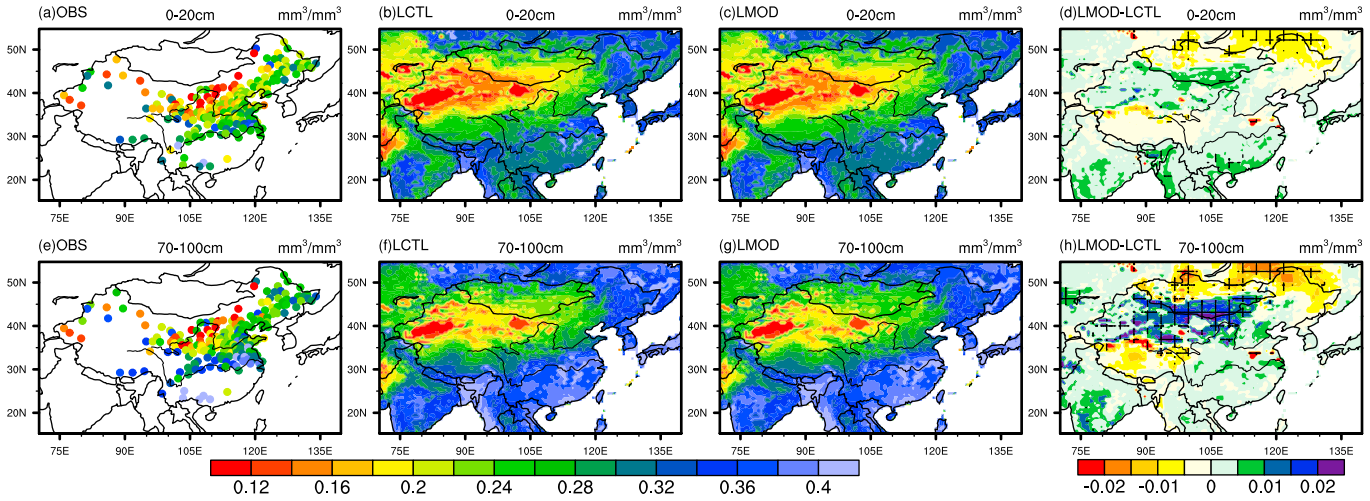

Figure 4. Same as Figure 3 but for the offline simulations.

in closer agreement with observations. The differences over northwestern China and the Tibetan Plateau increase in magnitude with depth, and regions with statistically significant differences at the 95% confidence level expand with depth (Figures 3d and 3h).

To better understand the effects of atmospheric feedback to soil moisture in coupled simulations due to the modified Richards equation, Figure 4 shows the soil moisture results of offline simulations. Both LCTL and LMOD runs also succeed in capturing the observed spatial distribution in each observed layer (Figures 4b and 4f), but LCTL shows a positive bias over northeastern China and a negative bias over northwestern China, which is consistent with the results of *Wang and Zeng* [2011]. LMOD reduces the underestimation over northwestern China and the overestimation over part of northeastern China to some extent, but it does not show improvements in central Inner Mongolia or the northeast plain (Figures 4d and 4h). Similar to coupled simulations, differences between LMOD and LCTL increase in magnitude with depth, and those in 70–100 cm over semiarid and arid regions (northwestern region and Tibetan Plateau) are statistically significant (Figures 4d and 4h).

The impact of the revised Richards equation on soil moisture in coupled simulations (Figures 3d and 3h) agrees with offline simulations over northwestern China and Tibetan Plateau, while it is different from offline simulations over eastern China. In fact, changes in soil moisture are intensified in coupled simulations over the arid and semiarid northwestern China and Tibetan Plateau, and they are geographically different from changes in offline simulations (Figures 4d and 4h) over the eastern monsoon area due to atmospheric responses. Over the eastern region, the biggest changes in soil moisture occur over the middle and lower reaches of Yangtze River and western northeast China in the coupled simulations (Figures 3d and 3h), yet the largest changes take place in a small part of north of the middle and lower reaches of Yangtze River and northern northeast China in the offline simulations (Figures 4d and 4h).

As shown in Figures 3 and 4, differences of soil moisture over most areas with adequate observation stations are small. To further compare simulated soil moisture with observed values, we select grid cells nearest to observation stations with differences between MOD and CTL in 70–100 cm larger than 0.01 mm^3/mm^3 (Figure 5). RMOD performs better than RCTL over the two layers, in terms of a slightly smaller root-mean-squared error (RMSE) and a slightly higher correlation. In contrast, LMOD has a slightly smaller RMSE, while LCTL has a slightly higher correlation over the two layers. On the other hand, the large soil moisture biases of LCTL in several grid boxes are reduced in LMOD (Figures 5c and 5d).

The mean vertical profiles of soil moisture in summer from offline and coupled simulations over the six subregions are shown in Figure 6. Clearly, the effect of the modified Richards equation on soil moisture is dependent on climate zones. Over all subregions, differences between LMOD and LCTL gradually increase in magnitude with depth due to direct interaction between soil column and groundwater. Changes in humid SE and SC subregions are similar, with slight increases above about 1 m and decreases below (Figures 6c and 6d).

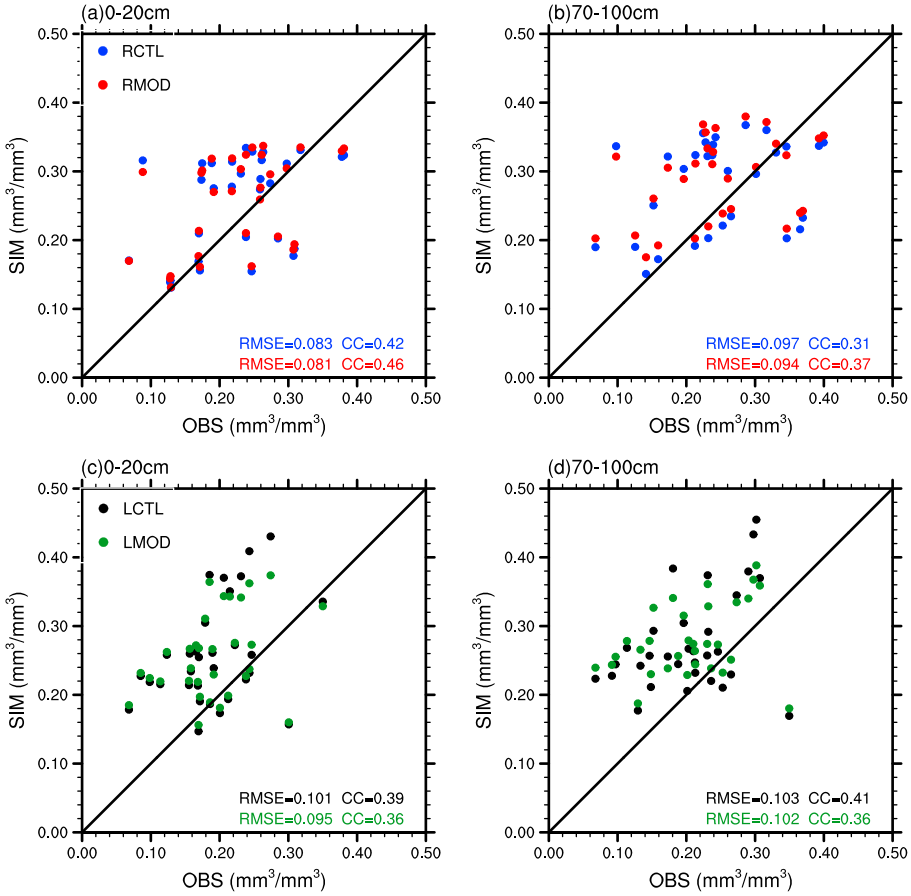

Figure 5. Comparison of mean soil moisture in JJA (1993–2001) at two layers (0–20 cm and 70–100 cm) simulated by (a, b) RCTL and RMOD, and (c, d) LCTL and LMOD, with in situ measurements. The root-mean-squared error (RMSE) and correlation coefficient values are provided in each panel.

As *Decker and Zeng* [2009] illustrated, modifying the Richards equation solves the problem of supersaturation below the water table and reallocation of the extra water, which could be one reason for the changes in the wet SE and SC subregions with water table depth of 1.4 m and 1.3 m, respectively (Figures 6c and 6d). The soil moisture differences in the semiarid TB subregion are negative in all model layers (Figure 6e). On the other hand, the arid NW subregion shows a wetter soil condition with the modified Richards equation (Figure 6f), partly because the modified method allows capillary pump of water from the aquifer to the soil column under dry conditions over these areas. In addition, changes in both semihumid NE and semiarid NC subregions are small (Figures 6a and 6b).

The change of soil moisture with depth is similar from LCTL and RCTL, but RCTL produces wetter soil in NE, NC, and NW subregions and dryer soil in SE and SC subregions compared to LCTL. Although precipitation from RCTL is less than that from LCTL over NW, soil column in RCTL is actually wetter as the atmospheric feedback is considered. The opposite occurs over SC. Over almost all subregions changes in vertical profiles of soil moisture in coupled simulations are in agreement with those in offline simulations, with the greatest differences in deep soil layers. The average (MOD − CTL) total column soil moisture differences double from offline to coupled simulations over TB (Table 3), but they are reduced over SE and SC. And the differences in coupled simulations are similar to those in offline simulations over NE and NW.

We have also compared the 0–20 cm soil moisture annual cycle from the four runs and observations averaged over the six subregions (figure not shown). The differences between RMOD and RCTL are larger than those between LMOD and LCTL in most months over all subregions because the atmospheric feedback is considered. RMOD generally decreases soil moisture over NE and NC, but increases soil moisture over SE and NW over almost all months with observations, resulting in simulated soil moisture closer to the observed values.

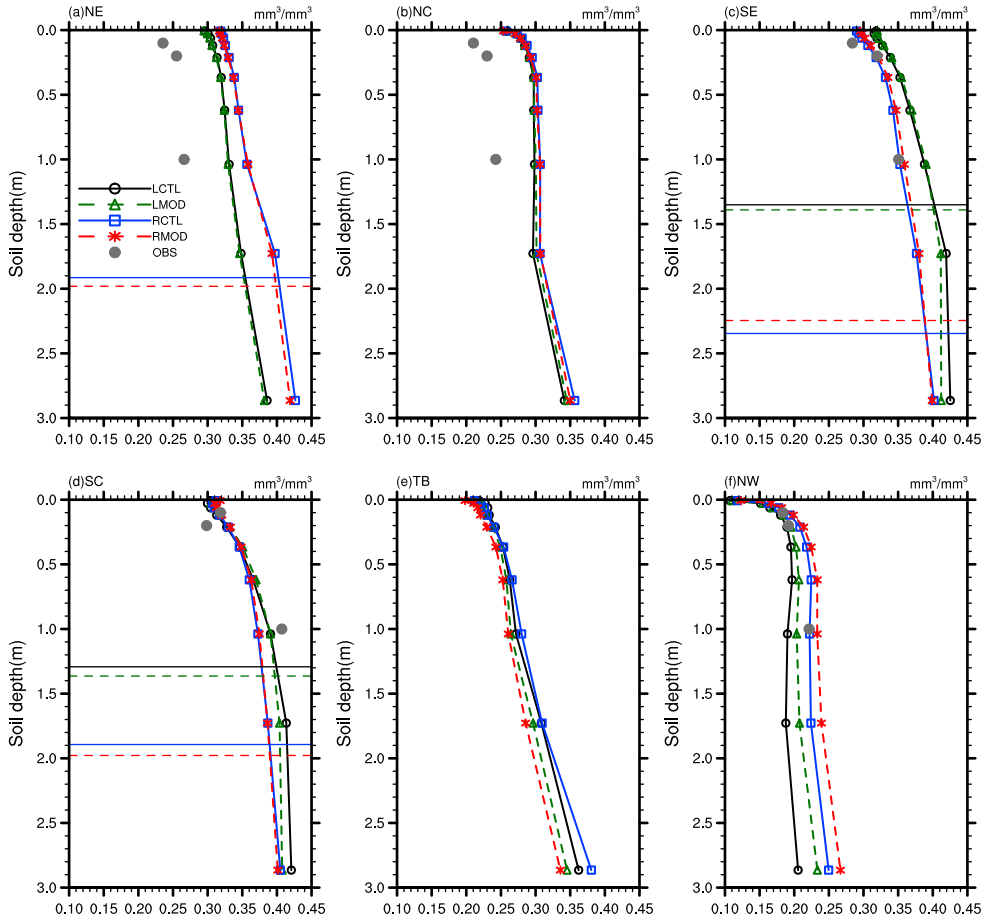

Figure 6. (a–f) Mean vertical profiles of soil moisture (1993–2001) in JJA from in situ observations, offline, and coupled simulations over the six subregions. Horizontal lines denote simulated mean water table depths.

Figure 7 evaluates the simulated monthly soil moisture anomalies with in situ measurements over SE and NW. Soil moisture temporal variations in both RCTL and LCTL are smaller than observations over both subregions especially for NW with the standard deviation (σ_{RCTL}) of ~0.010 versus σ_{OBS}~0.025 mm^3/mm^3 for all three layers (Figures 7d–7f). The damped variations are likely caused by the lack of consideration of irrigations in the model over large irrigated regions in eastern China and Hexi Corridor. Over SE, RCTL realistically shows the decrease of soil moisture standard deviation with depth (σ_{RCTL1} = 0.024, σ_{RCTL2} = 0.020, and σ_{RCTL3} = 0.015 mm^3/mm^3 versus σ_{OBS1} = 0.033, σ_{OBS2} = 0.028, and σ_{OBS3} = 0.020 mm^3/mm^3) (Figures 7a–7c). RMOD shows similar standard deviations as RCTL because of their high correlation ($\geq$ 0.8 for all three layers) over these two subregions (Figures 7a–7f). RMOD increases the correlation of soil moisture anomalies between coupled simulations and observations over SE from 0.24, 0.18, and 0.02 for the three layers in RCTL

Table 3. JJA (MOD-CTL) Differences of Subregion-Averaged Land Surface Water Cycle Variables[a]

Subregion	NE		NC		SE		SC		TB		NW	
Simulation	*R*	*L*	*R*	*L*	*R*	*L*	*R*	*L*	*R*	*L*	*R*	*L*
Total column soil water (mm^3/mm^3)	−0.01	−0.01	−0.01	0.01	0.01	−0.02	−0.00	−0.02	−0.09	−0.04	0.05	0.06
Evapotranspiration (mm/d)	−0.01	0.00	−0.02	0.01	−0.00	0.00	−0.02	0.02	−0.07	−0.03	0.06	0.04
Recharge rate (mm/d)	−0.06	0.01	−0.09	−0.01	0.27	0.01	−0.09	0.02	−0.03	0.03	0.02	−0.04
Water table depth (m)	0.07	0.08	0.26	0.12	−0.10	0.04	0.08	0.07	−0.71	−0.28	1.15	0.52
Precipitation (mm/d)	−0.09		−0.10		0.31		−0.09		−0.04		0.02	

[a]*R* and *L* denote results from coupled and offline simulations, respectively.

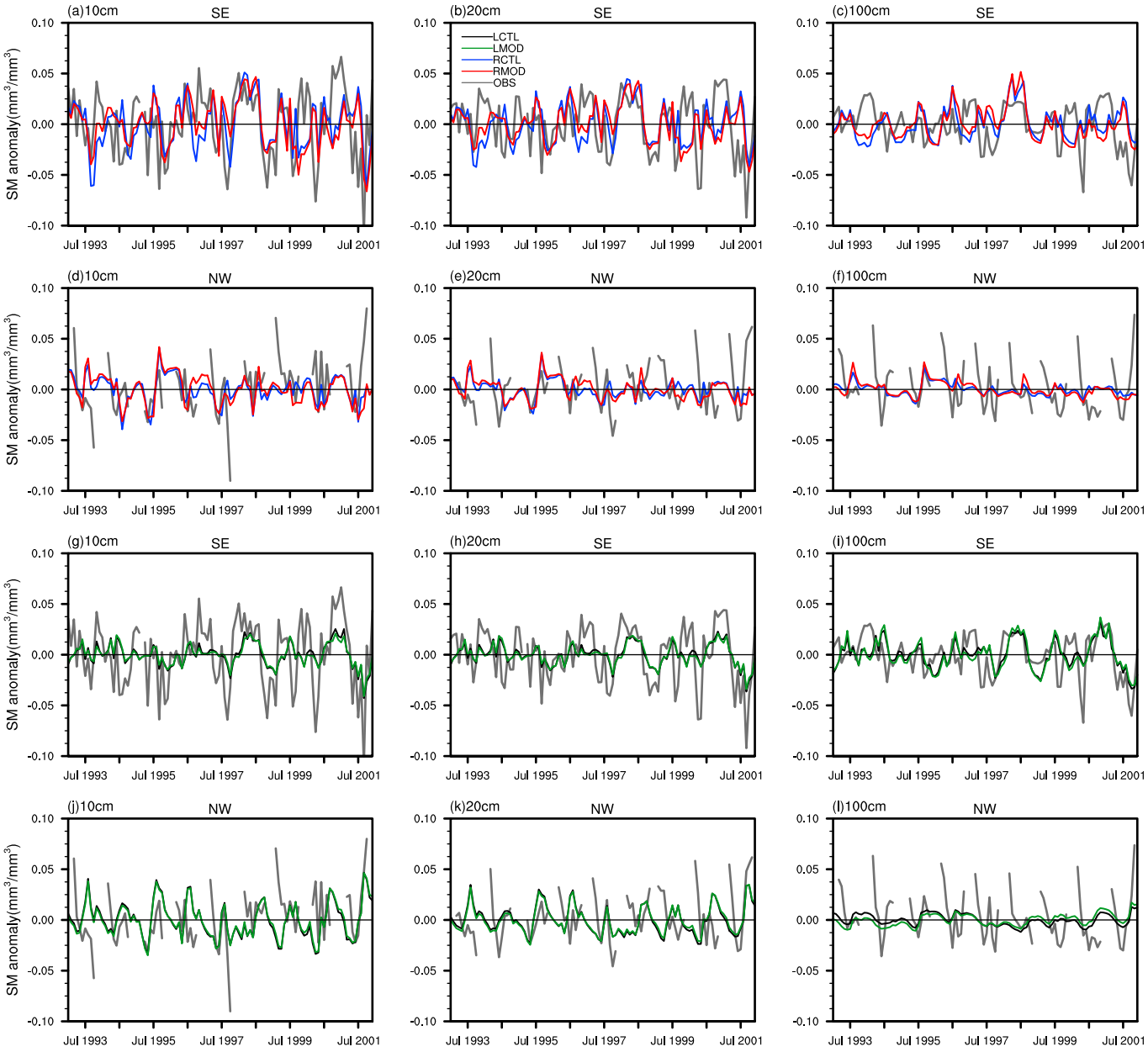

Figure 7. Observed and simulated monthly soil moisture anomalies (January 1993 to December 2001) averaged over observation stations in the SE and NW subregions at (a, d, g, j) 10 cm, (b, e, h, k) 20 cm, and (c, f, i, l) 100 cm depths. Results from RCTL and RMOD are shown in Figures 7a–7f, while results from LCTL and LMOD are shown in Figures 7g–7l.

to 0.28, 0.25, and 0.08. Over NW, correlation coefficients in RMOD are slightly better than those in RCTL only for the second layer (0.04 versus 0.10).

As shown in Figures 7g–7i, offline simulations show better correlation than coupled simulations over SE for the three layers, primarily due to atmospheric forcing data integrating observations (Tables 1 and 2). Compared with LCTL, LMOD improves the correlation with observations for the top two layers (0.14 versus 0.18 and 0.05 versus 0.09) over NW, without any improvements over SE. Because land-atmosphere interaction is considered in coupled simulations, soil moisture anomalies may result in changes in precipitation anomalies, which in turn may influence soil moisture anomalies. For instance, weakened negative precipitation anomalies lead to weakened negative soil moisture anomalies after July 1993 (Figure 7a), which is closer to the observed values.

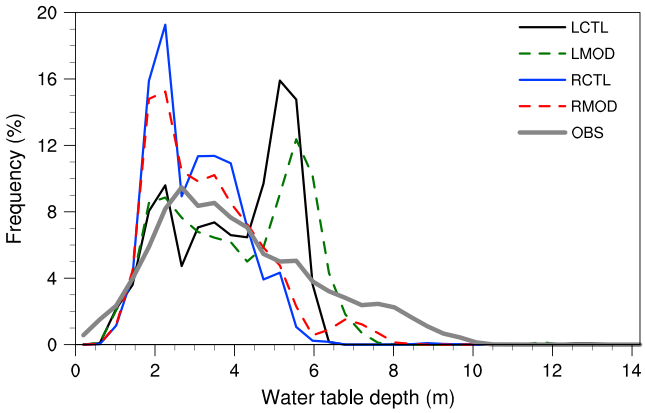

Figure 8. Histograms of the monthly water table depths (January 1993 to December 2001) from observations and model simulations.

The revised soil moisture scheme directly influences the water table depth due to direct coupling of groundwater with soil moisture. Here we interpolate model water table depth to individual wells by means of an inverse distance squared method. The frequency distributions of simulated and observed monthly water table depths over China are shown in Figure 8. Both offline simulations tend to overestimate the water table depth that occurs most frequently from ~3 m to ~5.5 m, even though the LMOD results fit the observed distribution slightly better. Both coupled runs more realistically simulate the water table depth that occur most frequently, but they significantly overestimate the frequency of the observed peak. RMOD reduces this overestimation and improves the overall frequency distribution of water table depth. Compared with RCTL and LCTL, RMOD and LMOD expand the maximum water table depth, in better agreement with observations.

4.3. Latent and Sensible Heat Fluxes

Changes in the calculated vertical distribution of soil moisture result from the modified Richards equation with the new lower boundary condition which directly couples groundwater with soil water and influences the land surface energy and water balance. Figure 9 shows the averaged diurnal cycle of latent heat flux from offline and coupled simulations in JJA. Over all subregions the diurnal phase of latent heat flux in coupled simulations is basically consistent with that in offline simulations, indicating the good performance of RegCM4 in simulating the diurnal cycle of precipitation, air temperature, and solar radiation flux. The diurnal amplitude in coupled simulations is larger than that in offline simulations over the NE, NC, SE, and SC subregions. Over semiarid TB and arid NW subregions, coupled runs show less latent heat flux than offline runs (Figures 9e and 9f). In contrast to the differences between offline and coupled runs, the (MOD − CTL) differences are generally much smaller in magnitude (with the peak differences near local noon from 0500 to 0800 UTC) mainly caused by small changes in near-surface soil moisture between MOD and CTL runs (Figure 6). For instance, the average difference between LMOD and LCTL is 0.9 W/m^2 from 0500 to 0800 UTC over SC, and the difference between RMOD and RCTL is just −2.2 W/m^2.

Similar to latent heat flux, coupled runs succeed in keeping the diurnal phase of sensible heat flux consistent with that in offline runs over all subregions and the diurnal peak of sensible heat flux differences due to the modified Richards equation also occurs near local noon for both offline and coupled simulations (not shown). For instance, the average sensible heat flux difference between LMOD and LCTL is approximately +1.3 W/m^2 from 0500 to 0800 UTC over TB, which is amplified to approximately +4.5 W/m^2 between RMOD and RCTL.

The detailed (MOD − CTL) changes in land surface water balance simulated by offline and coupled runs for the six subregions are presented in Table 3. Over NC and TB the negative (MOD − CTL) precipitation difference in coupled simulations leads to dryer soil and decreased evapotranspiration (ET). Over SE, in contrast, positive precipitation difference leads to wetter soil but slightly decreased ET, partly because ET is constrained by both soil moisture and surface net radiative flux in humid areas (such as SE with a decrease of 2.3 W/m^2 in surface net radiative flux). Indeed, the precipitation difference over SE primarily changes the recharge rather than ET or surface runoff (Table 3). Over both TB and NW, the (MOD − CTL) differences in ET are larger in coupled simulations than in offline simulations.

Recharge can be computed as precipitation minus surface runoff and evapotranspiration. Over NE, NC, SE, and SC, relatively strong land surface feedbacks to the atmosphere lead to relatively large (RMOD − RCTL) precipitation differences. This, in turn, results in larger recharge differences than those from offline simulations where the same atmospheric forcing is used over these subregions (Table 3). The modified Richards equation

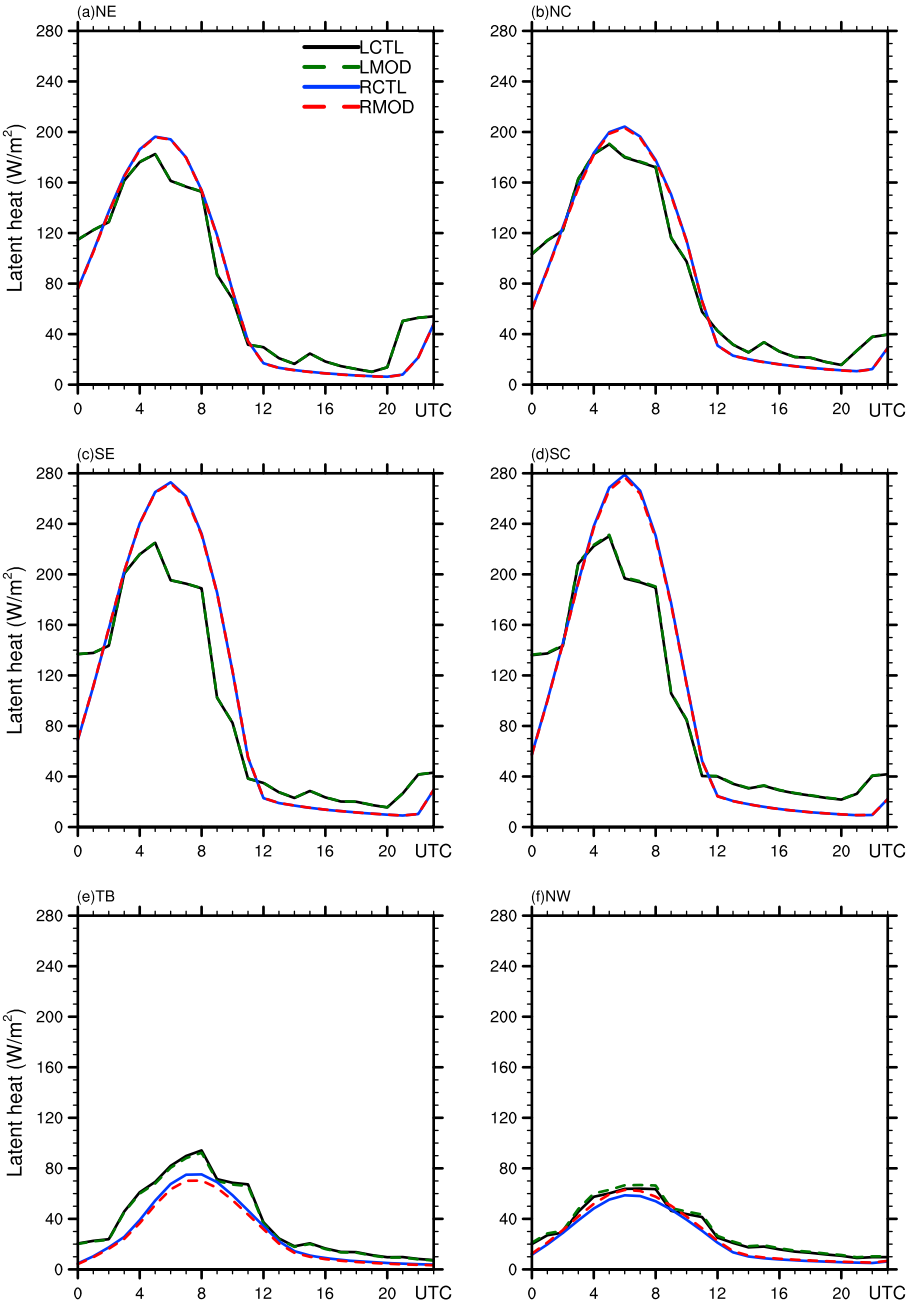

Figure 9. (a–f) Averaged diurnal cycle of latent heat flux from offline and coupled simulations in JJA from 1993–2001 over the six subregions.

usually enables more capillary pumping of water from the aquifer to the soil column, leading to positive (MOD − CTL) groundwater table depth differences over four of the six subregions (Table 3).

To further understand the above results, we have computed the differences of JJA mean total column soil moisture and water table depth between MOD and CTL as a function of precipitation with a 0.1 mm/d bin width in the CTL run using data over all grid cells in the study domain. The water table depth differences are primarily positive in both offline and coupled simulations, indicating the stronger capillary pumping of water from the aquifer to the soil column in MOD, as mentioned earlier. The soil moisture differences are primarily positive (or negative) for precipitation less than (or greater than) 2 mm/d in the offline simulations. For coupled simulations, the precipitation differences between RMOD and RCTL are primarily positive for

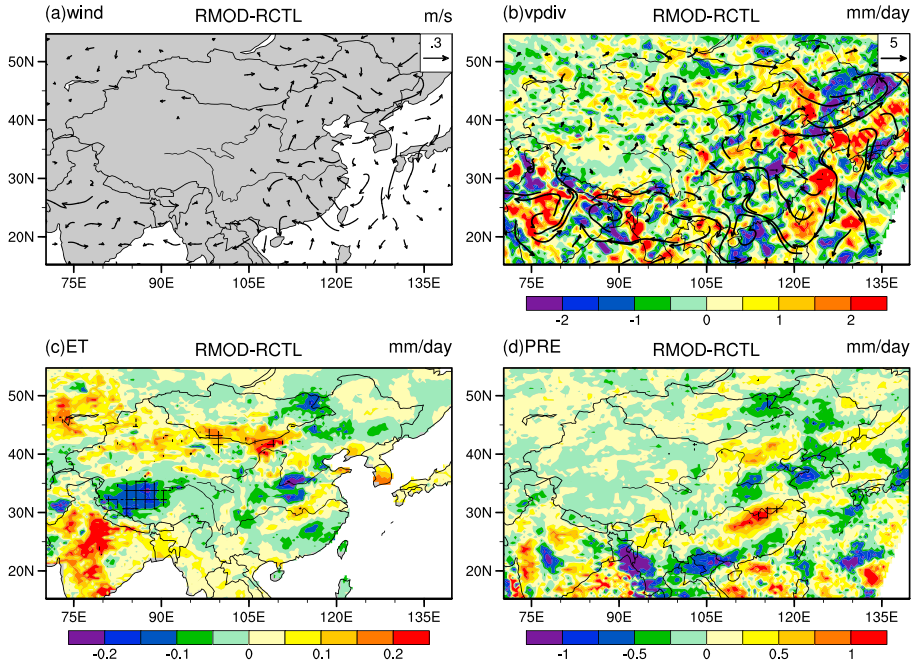

Figure 10. Mean differences in JJA (1993–2001) in (a) 850 hPa wind (m s^{-1}), (b) water vapor flux vector (kg m^{-1} s^{-1}) and its divergence (mm/d), (c) evapotranspiration (mm/d), and (d) precipitation (mm/d) between the RMOD and RCTL runs. Note that the color bars differ for various panels.

precipitation less than 2 mm/d and between 4 and 7.5 mm/d and primarily negative for other precipitation ranges. Because of these differences, the soil moisture differences in the coupled simulations become negative for precipitation between 0.5 and 4.5 mm/d and positive for other precipitation ranges. Over the semiarid NC subregion, for instance, these results explain the positive water table differences in both offline and coupled simulations but positive (or negative) soil moisture differences in offline (or coupled) simulations in Table 3.

4.4. Large-Scale Atmospheric Processes

In general, precipitation over an area is affected by local surface feedbacks (as emphasized so far) and large-scale moisture advection which itself is affected by surface-atmosphere interactions. Quantitatively, monthly or seasonal mean precipitation is balanced by surface evapotranspiration (ET), water vapor flux divergence ($\nabla \cdot \boldsymbol{Q}$), and the temporal variation of vertically integrated water vapor in the atmosphere (which is small relative to other terms at monthly or seasonal time scales). The vertically integrated water vapor flux vector $\boldsymbol{Q}$ is calculated from

$$\boldsymbol{Q} = \frac{1}{g}\int_{100}^{p_s} \boldsymbol{V} \cdot q \mathrm{d}p = \frac{1}{g}\int_{100}^{p_s} (u, v) \cdot q \mathrm{d}p \tag{8}$$

where u and v are zonal and meridional wind velocities (m/s), q is specific humidity (kg/kg), and p_s is surface pressure (hPa).

The spatial differences in JJA mean 850 hPa wind, $\boldsymbol{Q}$ and its divergence, evapotranspiration, and precipitation between RMOD and RCTL are shown in Figure 10. Changes in the 850 hPa wind fields display an anticyclonic anomaly over East China Sea, strengthening southeastern wind over southeast China (Figure 10a). The changes of circulation affect the water vapor transport. Changes in water vapor flux divergence are highly heterogeneous (Figure 10b). Decreases in evapotranspiration over the NE and SC subregions (Figure 10c) accompanied by moisture divergence result in decreases in precipitation (Figure 10d). Over the NC subregion both the moisture flux divergence tendency by 0.5 mm/d and decreased evapotranspiration by 0.02 mm/d contribute to decreased precipitation. Increased rainfall over the SE subregion (Figure 10d) is mainly caused by the southeastern wind anomaly (Figure 10a) which brings about moisture flux convergence (Figure 10b). Over most of the Tibetan Plateau region, the (RMOD − RCTL) ET differences are negative (Figure 10c). The

negative precipitation difference averaged over the TB subregion (−0.04 mm/d) is about half of the ET difference (−0.07 mm/d) (Table 3), because of the partial compensation from positive large-scale water vapor flux convergence difference (0.03 mm/d). On the contrary, the ET difference averaged over the NW subregion (0.06 mm/d) is 3 times as large as the precipitation difference (0.02 mm/d) (Table 3), mainly because of the positive moisture divergence difference (0.04 mm/d).

It is noted that significant (LMOD − LCTL) differences of soil moisture over the Tibetan Plateau in offline simulations are enhanced in coupled simulations (Figures 3 and 4), which can be attributed to atmospheric responses to changes in land surface condition. Figure 10b shows that the (RMOD − RCTL) differences in water vapor flux divergence are heterogeneous over this region. Qualitatively, the nonlinear mechanisms to explain the different results from offline and coupled simulations are as follows: most of this region (with negative (LMOD − LCTL) soil moisture differences in offline simulations) has negative (RMOD − RCTL) precipitation differences primarily due to negative ET, even though moisture flux convergence difference is positive. Subsequently, this leads to negative soil moisture differences and hence negative ET in coupled simulations. This in turn further decreases precipitation. Similarly, the ET differences in the offline simulations are enhanced in the coupled simulations over NW (Table 3). In other words, the modified Richards equation results in positive atmospheric feedbacks to changes in land surface condition over the arid northwestern region and semiarid Tibetan Plateau.

5. Conclusions

In this study, a revised numerical algorithm for solving the Richards equation is implemented in RegCM4 with its land surface component CLM3.5 to investigate its impact on regional climate modeling over East Asia. The modified numerical algorithm reduces the systematic error of RegCM4-simulated summer precipitation over southeast (SE), south China (SC), and northwest (NW), while it increases the error over three other subregions (northeast, north China, and Tibetan Plateau). The impact of the modified Richards equation on the simulated summer temperature is relatively small (with the mean biases changed by less than 10% over most regions in China).

Changes in soil moisture between RMOD and RCTL simulated by the regional climate model are enhanced over the Tibetan Plateau compared to offline simulations, and they are geographically different from those simulated by the offline land surface model over the eastern monsoon area due to land surface feedbacks to the atmosphere in the coupled simulations. Both coupled and offline simulations succeed in capturing the observed soil moisture spatial distribution. RMOD slightly reduces the root-mean-square errors and yields better spatial correlation with in situ measurements than RCTL. Soil moisture differences in coupled simulations are larger than those in offline simulations in most months and the annual cycle simulated by RMOD are closer to observation to some extent. In addition, RMOD yields better temporal correlation with observed soil moisture anomalies than RCTL over southeast China, while its standard deviation is similar that of RCTL.

Compared with in situ observations, the frequency distribution of water table depth is more realistically simulated in coupled runs than in offline runs. The modified Richards equation expands the maximum water table depth in both offline and coupled simulations, in better agreement with observations. The differences in the diurnal cycle of latent and sensible heat fluxes are small in both offline and coupled simulations, with the peak differences primarily occurring near local noon. In the coupled simulations, wetter soil and deeper water table depth are associated with increased precipitation over the northwest subregion, while dryer soil and shallower water table depth are associated with less precipitation over the Tibetan Plateau.

Monthly and seasonal (RMOD − RCTL) precipitation differences are primarily balanced by the differences in surface evapotranspiration (ET) and large-scale moisture flux convergence which itself is affected by land surface processes. These two terms have opposite signs over the arid northwest subregion and semiarid Tibetan Plateau. The (LMOD − LCTL) soil moisture and ET differences in offline simulations over the Tibetan Plateau are enhanced in coupled simulations because of the land-atmosphere interactions. Similarly, the ET differences in the offline simulations are enhanced in the coupled simulations over the northwest subregion. Furthermore, the ET differences over these subregions are greater in magnitude than the precipitation differences in coupled simulations because of the compensating large-scale moisture flux divergence. Therefore, both offline and coupled simulations are needed to fully understand the impact of the modified

Richards equation on land surface and atmospheric processes, as done in this study. Furthermore, numerical experiments here also provide preliminary tests for coupling the Community Land Model CLM4.5, which uses the modified Richards equation proposed in *Zeng and Decker* [2009], into the regional climate model RegCM4.

It should be noted that the modified Richards equation results in only moderate changes in precipitation, and to some extent, 2 m air temperature. Such changes do not pass the statistical significance test at 95% confidence level over most of the study domain. Soil moisture changes are also moderate. Only the water table depth simulation shows a relatively consistent improvement using the revised Richards equation. Recognizing that the land-atmosphere coupling strength over East Asia is weaker than some other regions such as part of the North America [*Koster et al*., 2004], an interesting question is whether the changes due to the modified Richards equation would be larger over these regions (with stronger land-atmosphere coupling strength).

Human activities such as irrigation and groundwater pumping are extensive over East Asia (e.g., north China), but they are not included in this study. They have a significant influence on hydrologic simulations [*Haddeland et al*., 2006; *Wada et al*., 2011; *Pokhrel et al*., 2012]. Moreover, surface energy balance is significantly affected in irrigated areas as a result of increased latent heat flux. For instance, over semiarid regions (e.g., north China), irrigation would increase surface evapotranspiration and precipitable water in the atmosphere, which are likely increase precipitation. This would reduce the precipitation underestimation in the coupled simulations (Table 1). Therefore, it is important to incorporate human activities in large-scale land surface and climate models in future studies.

Acknowledgments

This research was supported by the National Natural Science Foundation of China (grant 91125016) and the Chinese Academy of Sciences Strategic Priority Research Program (grant XDA05110102). The work of X.Z. was supported by the National Science Foundation (AGS-0944101). We would like to thank Feng Chen for helpful discussion and three anonymous reviewers for their constructive comments and suggestions. Six hour ERA-40 reanalysis data are acquired from http://users.ictp.it/~pubregcm/RegCM4/globedat.htm. Precipitation observations in this paper are adopted from *Xie et al.* [2007], 2 m air temperature data are from *Mitchell and Jones* [2005], and Princeton atmospheric forcing are provided by *Sheffield et al.* [2006]. Situ observations of soil moisture are available from China Meteorological Data Sharing Service System (http://cdc.cma.gov.cn/home.do).

References

Anyah, R. O., C. P. Weaver, G. Miguez-Macho, Y. Fan, and A. Robock (2008), Incorporating water table dynamics in climate modeling: 3. Simulated groundwater influence on coupled land-atmosphere variability, *J. Geophys. Res.*, *113*, D07103, doi:10.1029/2007JD009087.

Chen, F., and J. Dudhia (2001), Coupling an advanced land surface-hydrology model with the Penn State-NCAR MM5 modeling system. Part I: Model implementation and sensitivity, *Mon. Weather Rev.*, *129*(4), 569–585.

Chen, F., and Z. H. Xie (2010), Effects of interbasin water transfer on regional climate: A case study of the Middle Route of the South-to-North Water Transfer Project in China, *J. Geophys. Res.*, *115*, D11112, doi:10.1029/2009JD012611.

Chen, F., and Z. H. Xie (2012), Effects of crop growth and development on regional climate: A case study over East Asian monsoon area, *Clim. Dyn.*, *38*, 2291–2305, doi:10.1007/s00382-011-1125-y.

Chen, H. S., M. M. Xiong, and W. Y. Sha (2010), Simulation of land surface processes over China and its validation. Part I: Soil temperature [in Chinese], *Sci. Meteorol. Sin.*, *30*(5), 621–630.

Clapp, R. B., and G. M. Hornberger (1978), Empirical equations for some soil hydraulic-properties, *Water Resour. Res.*, *14*(4), 601–604, doi:10.1029/WR014i004p00601.

Cuenca, R. H., M. Ek, and L. Mahrt (1996), Impact of soil water property parameterization on atmospheric boundary layer simulation, *J. Geophys. Res.*, *101*(D3), 7269–7277, doi:10.1029/95JD02413.

Davies, H. C., and R. E. Turner (1977), Updating prediction models by dynamical relaxation—Examination of technique, *Q. J. R. Meteorol. Soc.*, *103*(436), 225–245, doi:10.1002/qj.49710343602.

Decker, M., and X. Zeng (2009), Impact of modified Richards equation on global soil moisture simulation in the Community Land Model (CLM3.5), *J. Adv. Model. Earth Syst.*, *2*, doi:10.3894/james.2009.1.5.

Dickinson, R. E., A. Henderson-Sellers, and P. J. Kennedy (1993), Biosphere-Atmosphere Transfer Scheme (BATS) version 1e as coupled to the NCAR Community Climate Model, *NCAR Tech. Rep. TN-387+STR*, 72 pp., Natl. Cent. for Atmos. Res., Boulder, Colo.

Eltahir, E. A. B. (1998), A soil moisture rainfall feedback mechanism: 1. Theory and observations, *Water Resour. Res.*, *34*(4), 765–776, doi:10.1029/97WR03499.

Fan, Y., G. Miguez-Macho, C. P. Weaver, R. Walko, and A. Robock (2007), Incorporating water table dynamics in climate modeling: 1. Water table observations and equilibrium water table simulations, *J. Geophys. Res.*, *112*, D10125, doi:10.1029/2006JD008111.

Fritsch, J. M., and C. F. Chappell (1980), Numerical prediction of convectively driven mesoscale pressure systems. 1. Convective parameterization, *J. Atmos. Sci.*, *37*(8), 1722–1733, doi:10.1175/1520-0469(1980)037<1722:Npocdm>2.0.Co;2.

Gao, X. J., Z. C. Zhao, and F. Giorgi (2002), Changes of extreme events in regional climate simulations over East Asia, *Adv. Atmos. Sci.*, *19*(5), 927–942.

Gao, X. J., Y. Xu, Z. C. Zhao, J. S. Pal, and F. Giorgi (2006), On the role of resolution and topography in the simulation of East Asia precipitation, *Theor. Appl. Climatol.*, *86*(1–4), 173–185, doi:10.1007/s00704-005-0214-4.

Gao, X. J., Y. Shi, and F. Giorgi (2011), A high resolution simulation of climate change over China, *Sci. China Earth Sci.*, *54*(3), 462–472, doi:10.1007/s11430-010-4035-7.

Gao, X. J., Y. Shi, D. F. Zhang, J. Wu, F. Giorgi, Z. M. Ji, and Y. G. Wang (2012), Uncertainties in monsoon precipitation projections over China: Results from two high-resolution RCM simulations, *Clim. Res.*, *52*(1), 213–226.

Gao, X., Y. Shi, R. Song, F. Giorgi, Y. Wang, and D. Zhang (2008a), Reduction of future monsoon precipitation over China: Comparison between a high resolution RCM simulation and the driving GCM, *Meteorol. Atmos. Phys.*, *100*(1–4), 73–86.

Gao, Y. H., et al. (2008b), Enhancement of land surface information and its impact on atmospheric modeling in the Heihe River basin, northwest China, *J. Geophys. Res.*, *113*, D20S90, doi:10.1029/2008JD010359.

Giorgi, F., Y. Huang, K. Nishizawa, and C. B. Fu (1999), A seasonal cycle simulation over eastern Asia and its sensitivity to radiative transfer and surface processes, *J. Geophys. Res.*, *104*(D6), 6403–6423, doi:10.1029/1998JD200052.

Giorgi, F., et al. (2012), RegCM4: Model description and preliminary tests over multiple CORDEX domains, *Clim. Res.*, *52*(1), 7–29.

Grell, G., J. Dudhia, and D. R. Stauffer (1994), A description of the fifth generation Penn State/NCAR Mesoscale Model (MM5), *NCAR Tech. Rep. TN-398+STR*, 121 pp., Natl. Cent. for Atmos. Res., Boulder, Colo.

Grell, G. A. (1993), Prognostic evaluation of assumptions used by cumulus parameterizations, *Mon. Weather Rev.*, *121*(3), 764–787, doi:10.1175/1520-0493(1993)121<0764:Peoaub>2.0.Co;2.

Guo, Z. C., P. A. Dirmeyer, Z. Z. Hu, X. Gao, and M. Zhao (2006), Evaluation of the Second Global Soil Wetness Project soil moisture simulations: 2. Sensitivity to external meteorological forcing, *J. Geophys. Res.*, *111*, D22S03, doi:10.1029/2006JD007845.

Haddeland, I., D. P. Lettenmaier, and T. Skaugen (2006), Effects of irrigation on the water and energy balances of the Colorado and Mekong river basins, *J. Hydrol.*, *324*, 210–223, doi:10.1016/j.jhydrol.2005.09.028.

Kim, J. E., and S. Y. Hong (2007), Impact of soil moisture anomalies on summer rainfall over East Asia: A regional climate model study, *J. Clim.*, *20*(23), 5732–5743.

Koster, R. D., P. A. Dirmeyer, Z. C. Guo, G. Bonan, E. Chan, P. Cox, and C. T. Gordon (2004), Regions of strong coupling between soil moisture and precipitation, *Science*, *305*(5687), 1138–1140, doi:10.1126/science.1100217.

Lai, X., J. Wen, S. X. Ceng, H. Q. Song, H. Tian, X. K. Shi, Y. He, and X. Huang (2014), Numerical simulation and evaluation study of soil moisture over China by using CLM4.0 model [in Chinese], *J. Atmos. Sci.*, *38*(3), 499–512.

Lawrence, D. M., et al. (2011), Parameterization improvements and functional and structural advances in version 4 of the Community Land Model, *J. Adv. Model. Earth Syst.*, *3*, doi:10.1029/2011MS000045.

Lawrence, D. M., K. W. Oleson, M. G. Flanner, C. G. Fletcher, P. J. Lawrence, S. Levis, S. C. Swenson, and G. B. Bonan (2012), The CCSM4 land simulation, 1850–2005: Assessment of surface climate and new capabilities, *J. Clim.*, *25*(7), 2240–2260.

Lawrence, P. J., and T. N. Chase (2007), Representing a new MODIS consistent land surface in the Community Land Model (CLM 3.0), *J. Geophys. Res.*, *112*, G01023, doi:10.1029/2006JG000168.

LeMone, M. A., F. Chen, J. G. Alfieri, M. Tewari, B. Geerts, Q. Miao, R. L. Grossman, and R. L. Coulter (2007), Influence of land cover and soil moisture on the horizontal distribution of sensible and latent heat fluxes in southeast Kansas during IHOP_2002 and CASES-97, *J. Hydrometeorol.*, *8*(1), 68–87.

Li, H. B., A. Robock, S. X. Liu, X. G. Mo, and P. Viterbo (2005), Evaluation of reanalysis soil moisture simulations using updated Chinese soil moisture observations, *J. Hydrometeorol.*, *6*(2), 180–193.

Li, L. H., L. Bai, Y. N. Yao, Q. Yang, and X. Zhao (2013), Patterns of climate change in Xinjiang projected by IPCC SRES, *J. Resour. Ecol.*, *4*(1), 27–35, doi:10.5814/j.issn.1674-764x.2013.01.004.

Li, M. X., and Z. G. Ma (2010), Comparisons of simulations of soil moisture variations in the Yellow River basin driven by various atmospheric forcing data sets, *Adv. Atmos. Sci.*, *27*(6), 1289–1302, doi:10.1007/s00376-010-9155-7.

Liang, X., Z. H. Xie, and M. Y. Huang (2003), A new parameterization for surface and groundwater interactions and its impact on water budgets with the variable infiltration capacity (VIC) land surface model, *J. Geophys. Res.*, *108*(D16), 8613, doi:10.1029/2002JD003090.

Liu, J. G., and Z. H. Xie, (2013), Improving simulation of soil moisture in China using a multiple meteorological forcing ensemble approach, *Hydrol. Earth Syst. Sci.*, *17*, 3355–3369 doi:10.5194/hess-17-3355-2013.

Liu, S. X., X. G. Mo, H. B. Li, G. B. Peng, and A. Robock (2001), Spatial variation of soil moisture in China: Geostatistical characterization, *J. Meteorol. Soc. Japan*, *79*(1B), 555–574.

Liu, S. Y., W. Gao, and X. Z. Liang (2013), A regional climate model downscaling projection of China future climate change, *Clim. Dyn.*, *41*(7–8), 1871–1884, doi:10.1007/s00382-012-1632-5.

Liu, Y. Q., F. Giorgi, and W. M. Washington (1994), Simulation of summer monsoon climate over East-Asia with an NCAR Regional Climate Model, *Mon. Weather Rev.*, *122*(10), 2331–2348.

Maxwell, R. M., J. K. Lundquist, J. D. Mirocha, S. G. Smith, C. S. Woodward, and A. F. B. Tompson (2011), Development of a coupled groundwater-atmosphere model, *Mon. Weather Rev.*, *139*(1), 96–116.

Miguez-Macho, G., and Y. Fan (2012), The role of groundwater in the Amazon water cycle: 1. Influence on seasonal streamflow, flooding and wetlands, *J. Geophys. Res.*, *117*, D15113, doi:10.1029/2012JD017539.

Miguez-Macho, G., Y. Fan, C. P. Weaver, R. Walko, and A. Robock (2007), Incorporating water table dynamics in climate modeling: 2. Formulation, validation, and soil moisture simulation, *J. Geophys. Res.*, *112*, D13108, doi:10.1029/2006JD008112.

Milly, P. C. D. (1992), Potential evaporation and soil-moisture in general-circulation models, *J. Clim.*, *5*(3), 209–226, doi:10.1175/1520-0442(1992)005<0209:Peasmi>2.0.Co;2.

Mitchell, K. E., et al. (2004), The multi-institution North American Land Data Assimilation System (NLDAS): Utilizing multiple GCIP products and partners in a continental distributed hydrological modeling system, *J. Geophys. Res.*, *109*, D07S90, doi:10.1029/2003JD003823.

Mitchell, T. D., and P. D. Jones (2005), An improved method of constructing a database of monthly climate observations and associated high-resolution grids, *Int. J. Climatol.*, *25*(6), 693–712.

Niu, G. Y., Z. L. Yang, R. E. Dickinson, L. E. Gulden, and H. Su (2007), Development of a simple groundwater model for use in climate models and evaluation with Gravity Recovery and Climate Experiment data, *J. Geophys. Res.*, *112*, D07103, doi:10.1029/2006JD007522.

Niu, G. Y., et al. (2011), The community Noah land surface model with multiparameterization options (Noah-MP): 1. Model description and evaluation with local-scale measurements, *J. Geophys. Res.*, *116*, D12109, doi:10.1029/2010JD015139.

Oleson, K. W., et. al. (2004), Technical description of the Community Land Model (CLM), *NCAR Tech. Rep.*, 174 pp., Natl. Cent. for Atmos. Res., Boulder, Colo.

Oleson, K. W., et al. (2008), Improvements to the Community Land Model and their impact on the hydrological cycle, *J. Geophys. Res.*, *113*, G01021, doi:10.1029/2007JG000563.

Pal, J. S., et al. (2007), Regional climate modeling for the developing world—The ICTP RegCM3 and RegCNET, *Bull. Am. Meteorol. Soc.*, *88*(9), 1395–1409, doi:10.1175/Bams-88-9-1395.

Pielke, R. A., J. Adegoke, A. Beltran-Przekurat, C. A. Hiemstra, J. Lin, U. S. Nair, D. Niyogi, and T. E. Nobis (2007), An overview of regional land-use and land-cover impacts on rainfall, *Tellus-B*, *59*(3), 587–601.

Pokhrel, Y., N. Hanasaki, S. Koirala, J. Cho, P. J. F. Yeh, H. Kim, S. Kanae, and T. Oki (2012), Incorporating anthropogenic water regulation modules into a land surface model, *J. Hydrometeorol.*, *13*(1), 255–269.

Reynolds, R. W., N. A. Rayner, T. M. Smith, D. C. Stokes, and W. Q. Wang (2002), An improved in situ and satellite SST analysis for climate, *J. Clim.*, *15*(13), 1609–1625.

Richards, L. A. (1931), Capillary conduction of liquids through porous mediums, *J. Appl. Phys.*, *1*(5), 318–333.

Schar, C., D. Luthi, U. Beyerle, and E. Heise (1999), The soil-precipitation feedback: A process study with a regional climate model, *J. Clim.*, *12*(3), 722–741.

Segal, M., Z. Pan, R. W. Turner, and E. S. Takle (1998), On the potential impact of irrigated areas in North America on summer rainfall caused by large-scale systems, *J. Appl. Meteorol.*, *37*(3), 325–331.

Sellers, P. J., D. A. Randall, G. J. Collatz, J. A. Berry, C. B. Field, D. A. Dazlich, C. Zhang, G. D. Collelo, and L. Bounoua (1996), A revised land surface parameterization (SiB2) for atmospheric GCMs. 1. Model formulation, *J. Clim.*, *9*(4), 676–705.

Sheffield, J., G. Goteti, and E. F. Wood (2006), Development of a 50-year high-resolution global dataset of meteorological forcings for land surface modeling, *J. Clim.*, *19*(13), 3088–3111, doi:10.1175/Jcli3790.1.

Syed, F. S., W. Iqbal, A. A. B. Syed, and G. Rasul (2014), Uncertainties in the regional climate models simulations of South-Asian summer monsoon and climate change, *Clim. Dyn.*, *42*(7–8), 2079–2097, doi:10.1007/s00382-013-1963-x.

Tawfik, A. B., and A. L. Steiner (2011), The role of soil ice in land-atmosphere coupling over the United States: A soil moisture-precipitation winter feedback mechanism, *J. Geophys. Res.*, *116*, D02113, doi:10.1029/2010JD014333.

Tian, W., X. Li, G. D. Cheng, X. S. Wang, and B. X. Hu (2012), Coupling a groundwater model with a land surface model to improve water and energy cycle simulation, *Hydrol. Earth Syst. Sci.*, *16*(12), 4707–4723.

Timbal, B., S. Power, R. Colman, J. Viviand, and S. Lirola (2002), Does soil moisture influence climate variability and predictability over Australia?, *J. Clim.*, *15*(10), 1230–1238.

Uppala, S. M., et al. (2005), The ERA-40 re-analysis, *Q. J. R. Meteorol. Soc.*, *131*(612), 2961–3012, doi:10.1256/Qj.04.176.

Wada, Y., L. P. H. van Beek, D. Viviroli, H. H. Dürr, R. Weingartner, and M. F. P. Bierkens (2011), Global monthly water stress: 2. Water demand and severity of water stress, *Water Resour. Res.*, *47*, W07518, doi:10.1029/2010WR009792.

Wang, A. H., and X. B. Zeng (2011), Sensitivities of terrestrial water cycle simulations to the variations of precipitation and air temperature in China, *J. Geophys. Res.*, *116*, D02107, doi:10.1029/2010JD014659.

Wu, J. (2012), Regional climate change simulations and uncertainty analysis over CORDEX-East Asia region [in Chinese], *Chinese Academy of Meteorological Sciences Doctor Degree Thesis*.

Wu, L. Y., and J. Y. Zhang (2013), Role of land-atmosphere coupling in summer droughts and floods over eastern China for the 1998 and 1999 cases, *Chin. Sci. Bull.*, *58*(32), 3978–3985, doi:10.1007/s11434-013-5855-6.

Xie, P. P., A. Yatagai, M. Y. Chen, T. Hayasaka, Y. Fukushima, C. M. Liu, and S. Yang (2007), A Gauge-based analysis of daily precipitation over East Asia, *J. Hydrometeorol.*, *8*(3), 607–626, doi:10.1175/Jhm583.1.

Xiong, M. M., H. Chen, and M. Yu (2011), Simulation of land surface processes over China and its validation Part II: Soil moisture [in Chinese], *Sci. Meteorol. Sin.*, *31*(1), 1–10.

Yang, F. L., A. Kumar, and K. M. Lau (2004), Potential predictability of US summer climate with "perfect" soil moisture, *J. Hydrometeorol.*, *5*(5), 883–895, doi:10.1175/1525-7541(2004)005<0883:Ppousc>2.0.Co;2.

Yu, Y., and Z. H. Xie (2013), A simulation study on climate effects of land cover change in China, *Adv. Clim. Change Res.*, *4*(2), 117–126, doi:10.3724/SP.J.1248.2013.117.

Yuan, X., Z. H. Xie, J. Zheng, X. J. Tian, and Z. L. Yang (2008a), Effects of water table dynamics on regional climate: A case study over East Asian monsoon area, *J. Geophys. Res.*, *113*, D21112, doi:10.1029/2008JD010180.

Yuan, X., Z. H. Xie, and M. Liang (2008b), Spatiotemporal prediction of shallow water table depths in continental China, *Water Resour. Res.*, *44*, W04414, doi:10.1029/2006WR005453.

Zeng, X. B., and M. Decker (2009), Improving the numerical solution of soil moisture-based Richards equation for land models with a deep or shallow water table, *J. Hydrometeorol.*, *10*(1), 308–319, doi:10.1175/2008jhm1011.1.

Zou, J., and Z. H. Xie (2012), The effects of the land-surface process parameterization of the RegCM4 on climate simulation in East Asia [in Chinese], *Acta Meteorol. Sin.*, *70*(6), 1312–1326.